Analytical noncovalent electrochemistry for battery engineering

Check for updates

Chang-Xin Zhao[1,2,3], Xi-Yao Li [2], Han Han[1,4], Yuanning Feng [1], Chun Tang[1,4], Xuesong Li [1,5], Long Zhang [1], Charlotte L. Stern [1], Qiang Zhang [2] & J. Fraser Stoddart [1,4,6,7,8]

Despite the fact that noncovalent bonding interactions are ubiquitous, it is primarily those interactions, which are amenable to spectroscopic analysis, that have been well investigated and applied in chemical engineering. New principles and techniques for characterizing noncovalent interactions are required to gain insight into their detailed nature and explore their potential applications. Here we introduce the practice of analytical noncovalent electrochemistry for probing such interactions. The strengths of noncovalent interactions can be determined more accurately by electrochemical means than by relying on spectroscopic measurements. Specifically, electrochemical analyses are capable of recording/identifying minor signals, leading to the discovery of an unexpected 2:1 host–guest complex. Moreover, the proposed technique is capable of probing multiple properties and facilitates the design and screening of active complexes as catalysts. We also demonstrate achieving a high energy density of 495 Wh kg^{-1} in rechargeable batteries. The analytical procedure provides a fresh perspective for supramolecular science and takes noncovalent chemistry closer to practical applications.

Noncovalent bonding interactions are ubiquitous in the natural world, exerting a pivotal influence on the maintenance of dynamic supramolecular and biological functions within DNA[1,2], proteins[3] and various other biomacromolecules[4]. These interactions have bestowed on us the capability to fabricate artificial molecular machines[5–8], consequently granting us fine control over the properties of materials at the molecular level. Moreover, they constitute an additional manifestation of chemical bonding, potentially introducing a fresh dimension of regulation into the realm of chemical engineering. In an attempt to unravel and scrutinize these noncovalent interactions, a multitude of characterization methodologies that are primarily dependent on spectroscopic techniques have been utilized. Among these techniques,

ultraviolet–visible[9] (UV–vis) and fluorescence emission spectroscopies[10] are prominent, collectively constituting the established bedrock of noncovalent spectroscopies. Nevertheless, the applicability of noncovalent spectroscopies is somewhat constricted as these characterization methods hinge on specific superstructures to elicit spectroscopic responses. It is thus imperative to establish alternative tools for the characterization of noncovalent bonding interactions, as well as to introduce methodologies that extend the repertoire beyond the current paradigms.

In addition to these conventional spectroscopic techniques, electrochemical signals obtained via cyclic voltammetry (CV) and differential pulse voltammetry (DPV) have also been integrated[11] into

[1]Department of Chemistry, Northwestern University, Evanston, IL, USA. [2]Tsinghua Center for Green Chemical Engineering Electrification, Beijing Key Laboratory of Green Chemical Reaction Engineering and Technology, Department of Chemical Engineering, Tsinghua University, Beijing, China. [3]Department of Chemical and Biomolecular Engineering, University of Maryland, College Park, MD, USA. [4]Department of Chemistry, The University of Hong Kong, Hong Kong, China. [5]Department of Chemistry, University of Wyoming, Laramie, WY, USA. [6]School of Chemistry, University of New South Wales, Sydney, New South Wales, Australia. [7]Stoddart Institute of Molecular Science, Department of Chemistry, Zhejiang University, Hangzhou, China. [8]ZJU-Hangzhou Global Scientific and Technological Innovation Center, Hangzhou, China. ✉e-mail: zhang-qiang@mails.tsinghua.edu.cn; stoddart@hku.hk
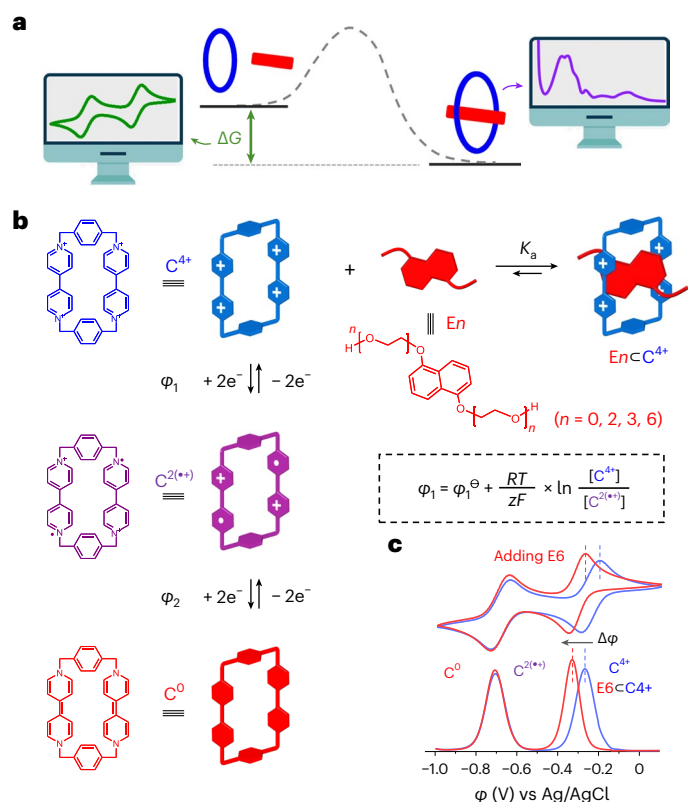
Fig. 1 | Electrochemical responses to noncovalent interactions. a, Schematic of different analytical methods for investigating noncovalent interactions featuring the proposed electrochemical strategy (left) and traditional spectroscopic characterization (right). The electrochemical signals are associated directly with various physicochemical properties and potentially minimize experimental errors during the evaluation of noncovalent interactions. **b**, The redox reactions summarized by $C^{4+}/C^{2(\bullet+)}/C^0$ (left) and the complexation between C^{4+} and En to form E$n \subset C^{4+}$ host–guest complexes (right). From the perspective of the Nernst equation (in the dashed box), the addition of En consumes C^{4+} and reduces the equilibrium potential (φ_1) for the $C^{4+}/C^{2(\bullet+)}$ redox couple. e$^-$, electron; $\varphi_1^\ominus$, standard potential; R, gas constant; T, absolute temperature; z, electron transfer number; F, Faraday constant. **c**, CV (top) and DPV (bottom) curves of 1.0 mM C^{4+} before (blue line) and after (red line) the addition of 2.0 mM E6. The electrochemical characterization was performed in acetonitrile (MeCN) with 0.1 M tetrabutylammonium hexafluorophosphate (TBAPF$_6$) as the supporting electrolyte and Ag/AgCl as the reference electrode. The peaks of $C^{4+}/C^{2(\bullet+)}$ shift to a lower potential, an observation that is consistent with the above theoretical analysis. By contrast, the peaks of $C^{2(\bullet+)}/C^0$ are not affected by the negligible interactions between En and $C^{2(\bullet+)}/C^0$.

the exploration of noncovalent bonding interactions. For instance, researchers have used the comparative analysis of redox peaks from complexes and their corresponding host/guest components[12,13]. This approach enables the identification of newly formed supramolecular entities, consequently implying the presence of noncovalent bonding interactions. Within this framework, however, the intricate connection between noncovalent interactions and electrochemistry remains largely unclarified, along with the underlying mechanisms and establishing titration methods in the case of analytical electrochemistry. For example, the strength of noncovalent interactions, quantified through binding constants (K_a) within host–guest complexes, has pivotal implications for both foundational investigations and practical applications[14–16]. The assessment of the strength of noncovalent interactions, however, has become dependent heavily on spectroscopic methods, whose signals possess a roughly linear relationship[17] (for example, the Lambert–Beer law) with respect to the concentration of the host or guest or their

complex, despite the fact that the accuracy[18,19] of these approaches has been less than satisfactory. Electrochemistry provides another perspective from which to study noncovalent interactions. Under the control of physicochemical laws, the thermodynamic potential is strictly and accurately related to the change in the Gibbs free energy (ΔG) caused by noncovalent interactions. Nevertheless, the quantification (such as through K_a values) of noncovalent interactions on the basis of electrochemical principles remains an area of relatively limited exploration. In essence, the interplay between noncovalent bonding interactions and electrochemistry, from the standpoint of analytical chemistry, is an emerging discipline (Fig. 1a) which has yet to be fully established.

If the quantitative relationship between noncovalent interactions and electrochemistry can be established from the standpoint of analytical chemistry, it could provide a new dimension for the precise control of electrochemical properties. For instance, in battery systems, the electrochemical properties of each component, including the electrodes, electrolytes and additives/catalysts, must be located precisely within narrow ranges to demonstrate the best battery performance. For instance, the redox potential of the redox mediator in oxygen- or sulfur-based cathodes must fall within a very narrow potential range to ensure that the catalytic process is thermodynamically feasible and kinetically favorable[20,21]. Therefore, if analytical noncovalent electrochemistry can be established, one should be able to modulate the electrochemical performance of battery systems by introducing and controlling the noncovalent interactions. Hence, it is an opportune time to introduce a systematic methodology for carrying out noncovalent electrochemical analysis and facilitating the development of application-oriented electrochemical engineering.

Results

Electrochemical responses to noncovalent interactions

We have selected a host–guest system to demonstrate the noncovalent electrochemical method of analysis. The host, cyclobis(paraquat-p-phenylene)[22,23] (C^{4+}), is a tetracationic cyclophane that contains two separate bipyridinium (BIPY^{2+}) units that are electrochemically active. C^{4+} (Fig. 1b, left) has two reduction potentials associated with its radical cationic ($C^{2(\bullet+)}$) and neutral (C^0) states[24], corresponding to the equilibrium potential (φ) values for the $C^{4+}/C^{2(\bullet+)}$ and $C^{2(\bullet+)}/C^0$ redox couples associated with φ_1 and φ_2, respectively. The thread-like guest consists of a naphthalene unit with appended $-(OCH_2CH_2)_nOH$ groups at its 1 and 5 positions, that is, En, where n refers to the number of repeating units present in the oligoethylene glycol chains. The donor–acceptor interactions between the BIPY^{2+} units in C^{4+} and the 1,5-dioxynaphthalene units in En are typical noncovalent interactions[25], which drive (Fig. 1b upper and Supplementary Figs. 4–8) the formation of the inclusion complexes (E$n \subset C^{4+}$). The $C^{2(\bullet+)}$ and C^0 states are relatively electron-rich and exhibit negligible interactions[26] with the En guests.

To establish a sound theoretical foundation for analytical noncovalent electrochemistry, we investigated the impact of noncovalent interactions on the electrochemical measurements. Upon the addition of En to the redox system of $C^{4+}/C^{2(\bullet+)}$, En combines selectively with C^{4+} to form host–guest complexes. As a result, the chemical potential (μ) of the oxidized species decreases, leading to a negative shift in the equilibrium potential (φ). Furthermore, the shifts in the equilibrium potential values can be rationalized by relating them to the concentrations of the redox components. With all the components in balance, we can determine the equilibrium potential using any of the redox couples in accordance with the Nernst equation. We have selected the $C^{4+}/C^{2(\bullet+)}$ redox system for investigation. Specifically, En consumes free C^{4+} and the concentration of free C^{4+} ([C^{4+}]) is reduced. According to the Nernst equation, the reduced [C^{4+}] leads to a reduction of the equilibrium potential from φ_1 to φ_1'. This analysis was confirmed by the CV and DPV curves in which the peaks for the $C^{4+}/C^{2(\bullet+)}$ redox system undergo a negative shift following the addition of En (Fig. 1c and Supplementary Fig. 11). Conversely, the peaks corresponding to the redox couple $C^{2(\bullet+)}/C^0$ remain unaffected since there are only weak interactions between
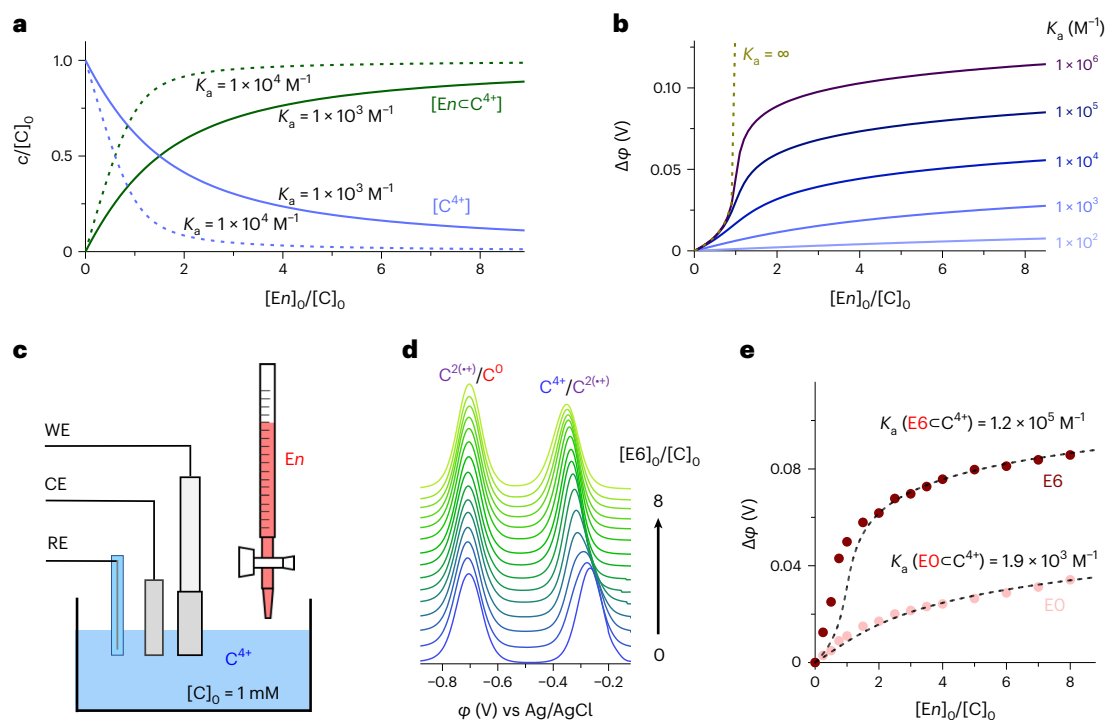
Fig. 2 | Electrochemical titrations. a, Titration of C^{4+} using En, showing the numerical simulation of the concentration of C^{4+} ($[C^{4+}]$, blue line) and $En \subset C^{4+}$ ($[En \subset C^{4+}]$, green line) with different K_a values, for $K_a = 10^3 \text{ M}^{-1}$ (solid line) and $K_a = 10^4 \text{ M}^{-1}$ (dashed line). The initial concentration of C^{4+} ($[C]_0$) is set to $[C]_0 = 1 \text{ mM}$. c, $[C^{4+}]$ or $[En \subset C^{4+}]$. **b**, Numerical simulation of the potential shift ($\Delta\varphi$) of $C^{4+}/C^{2(\bullet+)}$ at different En equivalents ($[En]_0/[C]_0$) and K_a values. The $\Delta\varphi–[En]_0/[C]_0$ curve is typically sigmoidal in shape with a titration jump at the equivalence point. Different K_a values correspond to distinct $\Delta\varphi–[En]_0/[C]_0$ curves, especially to the right of the equivalence point. **c**, Schematic of the setup used in the electrochemical titration by adding En to C^{4+}. WE, working electrode; CE, counter electrode; RE reference electrode. **d**, DPV curves at each En equivalent during the addition of 1.0 mM C^{4+} to E6, where $\Delta\varphi$ at each En equivalent was recorded. **e**, Measured $\Delta\varphi$ at different En equivalents during the electrochemical titration of C^{4+} with E0 (light red) or E6 (deep red), together with the fitting results (dashed lines) and the measured K_a values for E0$\subset C^{4+}$ and E6$\subset C^{4+}$. The anomalies in the theoretical and experimental electrochemical titration curves for titration with E6 imply the existence of 2:1 host–guest complexes.

En and $C^{2(\bullet+)}$ or C^0. The combination of theoretical and experimental results leads to the conclusion that electrochemical signals are able to serve as probes for detecting noncovalent interactions.

Measuring K_a values using electrochemical titrations

Using the Nernst relationship, the shift in equilibrium potential ($\Delta\varphi = \varphi_1 - \varphi_1'$, defined as the difference in equilibrium potential before and after the addition of En) can be expressed quantitatively as a function of the binding constant (K_a) and the guest/host ratio ($x = [En]_0/[C]_0$, defined as the En molar equivalent relative to C^{4+}). According to the stoichiometry of the complexation, the concentrations of free C^{4+} and $En \subset C^{4+}$ ($[C^{4+}]$ and $[En \subset C^{4+}]$, respectively) can be determined from the K_a values and $[En]_0/[C]_0$ (Fig. 2a). Furthermore, $\Delta\varphi$ can be calculated using the Nernst equation. The plot of $\Delta\varphi$ versus $[En]_0/[C]_0$ (Fig. 2b) is typically sigmoidal in shape with a sudden jump in the titration at the equivalence point when $[En]_0/[C]_0 = 1$. The reason for the jump is that $\Delta\varphi$ exhibits a logarithmic relationship with respect to $[C^{4+}]$, which undergoes a rapid change in its order of magnitude around the equivalence point. For systems with different K_a values (Fig. 2b), the titration curves in the range of $0 < [En]_0/[C]_0 < 1$ are similar, whereas they become distinct when $[En]_0/[C]_0 > 1$. The potential shift $\Delta\varphi$ has a positive correlation with the K_a value, especially in the case of the titration curve where the titration equivalent is greater than 1. By acquiring and fitting the titration curve, one can measure the K_a values of the host–guest complexes rather easily. The titrations were performed using an electrochemical cell (Fig. 2c and Supplementary Figs. 14–18) utilizing a micro-syringe to inject a specific amount of the En feedstock solution into 1 mM C^{4+}. With the increase in En equivalents during the titration, the redox potential of

$C^{4+}/C^{2(\bullet+)}$ showed a gradual negative shift whereas the redox potential of $C^{2(\bullet+)}/C^0$ remained unchanged (Fig. 2d and Supplementary Figs. 19 and 20). The potential shift $\Delta\varphi$ in the redox potential of $C^{4+}/C^{2(\bullet+)}$ at different titration steps was measured on the basis of the peak position changes in the DPV curves. By fitting the titration results, the K_a values of $En \subset C^{4+}$ ($n = 0, 2, 3, 6$) were measured and found to be 1.9×10^3, 1.9×10^4, 5.0×10^4 and $1.2 \times 10^5 \text{ M}^{-1}$, respectively (Fig. 2e and Supplementary Fig. 21). These binding constants are correlated positively with the lengths of the oligoethylene glycol chains in En, as a result of the enhanced [C–H⋯O] interactions[27] between C^{4+} and the oligoethylene glycol chains in En. These results, which are consistent with previously reported data[28], demonstrate the effectiveness of electrochemical titrations.

On the basis of the 1:1 binding model for the host–guest complex, the curve fitting of the E0$\subset C^{4+}$ titration agrees well with the experimental data. For the $En \subset C^{4+}$ titrations ($n = 2, 3, 6$), however, the curve fitting (Fig. 2e and Supplementary Fig. 21a), is not in good agreement with the experimental data in the interval of $0 < [En]_0/[C]_0 < 1$. Specifically, the recorded $\Delta\varphi$ in the range of $0 < [En]_0/[C]_0 < 1$ is higher than the theoretical maximum value of $\Delta\varphi$ corresponding to a K_a value of infinity. This result implies that the consumption of C^{4+} is greater than the theoretical maximum based on the 1:1 binding model. A possibility is that each En guest interacts with more than one C^{4+} host, forming a 2:1 host–guest complex, that is, a [3]pseudorotaxane ($En \subset 2C^{4+}$). Accordingly, we investigated a 2:1 host–guest model, where the first and second stepwise association constants are K_{a1} and K_{a2}, respectively (Fig. 3a). The overall association constant for the 2:1 host–guest complex is β_{21} ($\beta_{21} = K_{a1} \times K_{a2}$). The curve fitting (Fig. 3b) matches well with the experimental data across the full range of En equivalents, and the
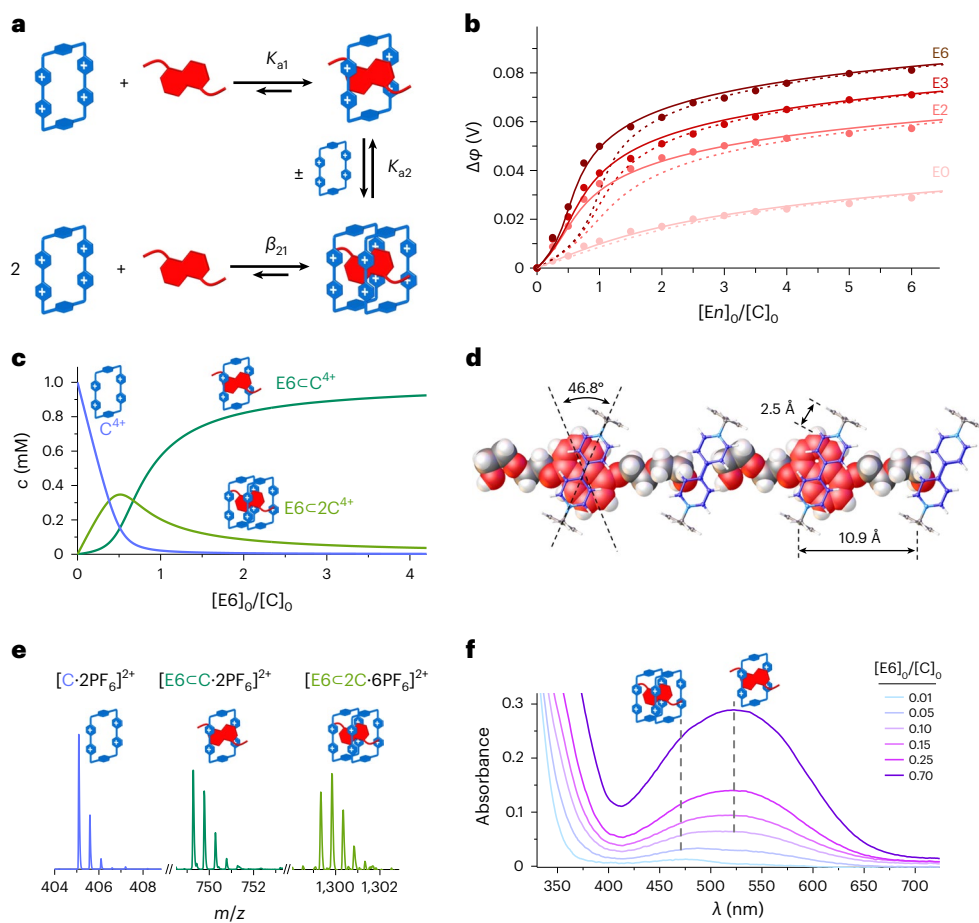
Fig. 3 | Discovering the 2:1 host–guest complex. a, Graphical representation of the proposed hypothesis, where a 2:1 host–guest complex (En⊂2C^{4+}) is formed during the initial titration stage. During this initial titration stage, C^{4+} is in excess with respect to En, a situation that is favorable for the formation of En⊂2C^{4+}. When more equivalents of En are added, En⊂2C^{4+} transforms into the En⊂C^{4+} 1:1 host–guest complex. **b**, Measured $\Delta\varphi$ at different En equivalents during electrochemical titration, together with the fitting results (solid lines) based on the model presented in **a**, where the formation of both En⊂C^{4+} and En⊂2C^{4+} host–guest complexes are taken into consideration. The dashed lines are the fitting results based on 1:1 binding model. **c**, Numerical simulation of the concentrations of C^{4+}, E6⊂C^{4+} and E6⊂2C^{4+} (with structures shown schematically as insets) at different equivalents of E6. The results show that the formation of En⊂2C^{4+} is favoured in the case of an excess of C^{4+}, inspiring us to search for evidence of the existence of En⊂2C^{4+} under the conditions where C^{4+} is in excess. **d**, Single-crystal superstructure of the En⊂2C^{4+} host–guest complex. The host–guest ratio was determined to be 2:1. MeCN solvent molecules and PF$_6^-$ counterions are omitted for clarity. **e**, Electrospray ionization mass spectra of the solution containing 1.0 mM C^{4+} and 0.2 mM E6, where the co-existence of C^{4+}, E6⊂C^{4+} and E6⊂2C^{4+} (shown as insets) can be observed. **f**, Evolution of the UV–vis spectra with the addition of E6 to 1 mM C^{4+} solution. The red-shift tendency (dashed line) indicates that the dominant species changes from E6⊂2C^{4+} (left inset) to E6⊂C^{4+} (right right) with the addition of E6.

values of K_{a1}, β_{21} and K_{a2} can be acquired. On the basis of the K_{a1} and K_{a2} values, the interaction parameter (α) for each En⊂2C^{4+} is calculated to be lower than 1, indicating that these systems display negative cooperativity. The concentrations of free C^{4+} and the En⊂C^{4+} and En⊂2C^{4+} complexes at different equivalents can also be calculated (Fig. 3c and Supplementary Fig. 27). The formation of En⊂2C^{4+} is dominant when the equivalence is lower than 1. When the En equivalence increases, the formation of the En⊂C^{4+} is more favorable.

Uncovering a 2:1 host–guest complex

On the basis of the results of the electrochemical titrations, we predicted that a 2:1 host–guest complex between C^{4+} and En can be formed. To confirm this prediction, single crystals were obtained by evaporating ^{i}Pr$_2$O into a solution of C^{4+} and En in MeCN with C^{4+} present in excess. Single-crystal X-ray diffraction analysis (Fig. 3d and Extended Data Fig. 1) demonstrated the formation of the 2:1 host–guest complex En⊂2C^{4+} in which one En guest is embraced by two C^{4+} host rings. We also observed the formation of En⊂2C^{4+} in the solution state, as shown using high-resolution electrospray ionization mass spectrometry (Fig. 3e). In a solution containing a mixture of C^{4+} and E6, the mass spectrum exhibited prominent peaks at mass-to-charge ratio (m/z) values of 405.0948, 749.2787 and 1,299.8397, in agreement with the calculated m/z values for [C·2PF$_6$]$^{2+}$, [E6⊂C·2PF$_6$]$^{2+}$ and [E6⊂2C·6PF$_6$]$^{2+}$, respectively. The formation of E2⊂2C^{4+} and E3⊂2C^{4+} was also confirmed (Supplementary Fig. 31) by mass spectrometry. The formation of these 2:1 host–guest complexes was also indicated using UV–vis spectroscopy (Fig. 3f). At a low En equivalents, the charge-transfer absorption bands were located at ~480 nm. When the En equivalents was increased, a new absorption band located at ~520 nm emerged and became dominant. According to time-dependent density functional theory calculations, the bands located at approximately 480 and 520 nm can be assigned to the 2:1 and 1:1 host–guest complexes, respectively (Supplementary Fig. 35). The red-shift in the wavelength (λ) arises from the fact that the proportion of the 1:1 complex gradually dominates that of the 2:1 complex with the increase in En equivalents. Furthermore, on the basis of the binding model associated with 1:1 and 2:1 host–guest equilibria, the UV–vis titration curves give a better fit when based on the binding model of the 1:1 host–guest equilibrium (Supplementary Fig. 34). These experimental results confirm our prediction of the formation of the 2:1 complex, demonstrating that the electrochemical analysis can, in some cases, provide more detailed
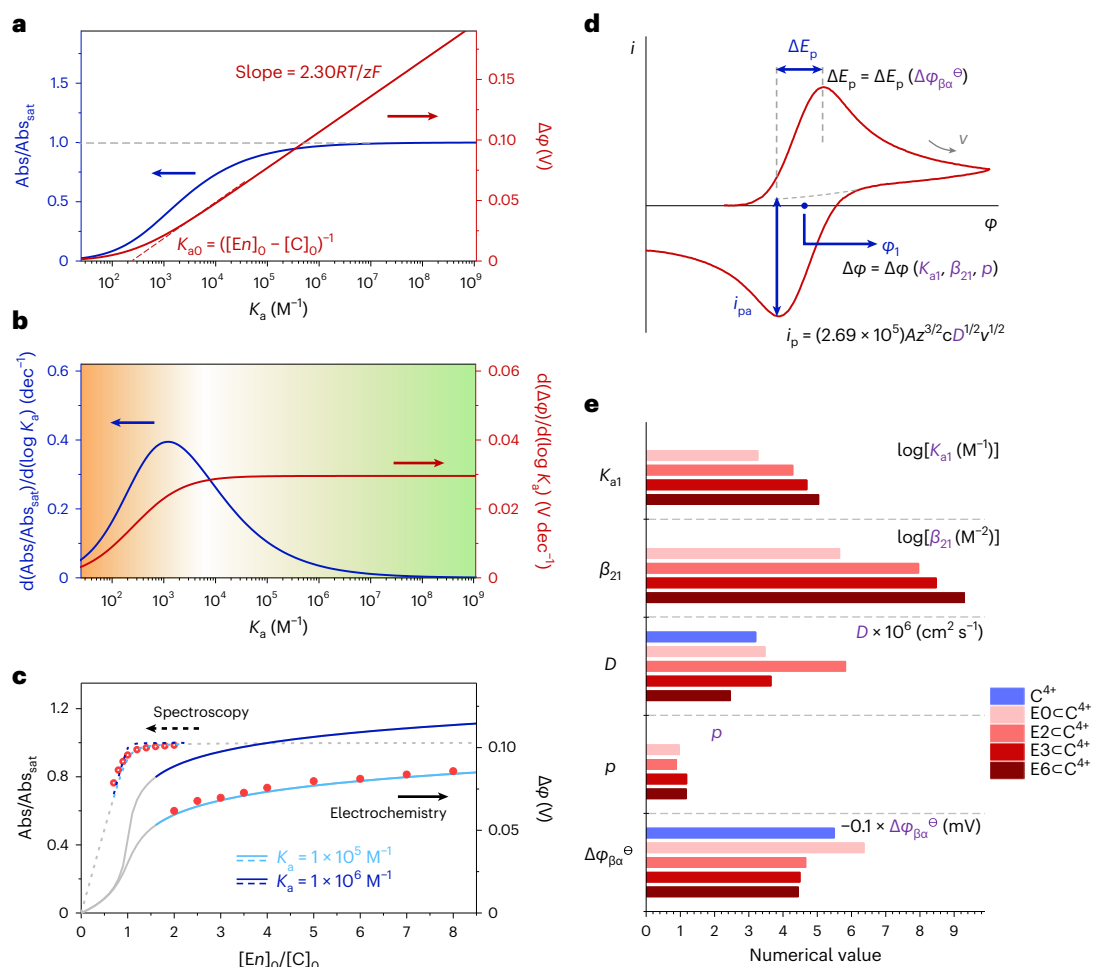
Fig. 4 | Advantages of the noncovalent electrochemical analysis.
a, Spectroscopic Abs/Abs$_{sat}$ signals and electrochemical $\Delta\varphi$ signals at different K_a values, where Abs and Abs$_{sat}$ denote the absorbance and saturation absorbance, respectively. Abs/Abs$_{sat}$ and $\Delta\varphi$ are collected at the En equivalents of 1.0 and 5.0, respectively. A higher tangential slope corresponds to a higher sensitivity in the variation of the K_a values. K_{a0} is the intercept of the asymptote of the red curve at the x axis. **b**, The differential curves of the data in **a**. A higher numerical value corresponds to a higher measurement accuracy. The electrochemical titration is more accurate when investigating host–guest complexes with larger K_a values. **c**, Numerical simulation of the UV–vis titration curves (dashed lines; left axis) and the electrochemical titration curves (solid lines; right axis) under different

K_a values, for $K_a = 1 \times 10^5$ M^{-1} (light blue lines) and $K_a = 1 \times 10^6$ M^{-1} (dark blue lines). The open red circles are the UV–vis titration results (left axis); the filled red circles are the electrochemical titration results (right axis). Both titrations were carried out by adding E6 to 1 mM C^{4+} solution. It is clear that the electrochemical titration is more accurate when measuring the K_a value of the E6⊂C^{4+} complex. **d**, The CV features of the host–guest complexes are determined via multiple properties, including K_a, D, p and $\Delta\varphi_{\beta\alpha}{}^{\ominus}$, which can be obtained through data digging. ΔE_p, change in peak potential; i_{pa}, anodic peak current; i_p, peak current; A, area of the WE; v, scan rate. **e**, Characteristic results of multiple properties of the host C^{4+} and its host–guest complexes acquired via electrochemical analysis.

information than traditional spectroscopic analysis because of the high sensitivity of the electrochemical signal with respect to the concentration. The traditional spectroscopic signals are correlated linearly with the absolute concentration, for example, the concentration of En⊂C^{4+} for the UV–vis spectra. By contrast, the electrochemical potential signal and the concentration are related logarithmically. Even a very small difference in concentration can therefore result in a large change in the potential.

Advantages of the noncovalent electrochemical method of analysis

The higher sensitivity of the electrochemical signal towards the concentration enables the accurate measurement of noncovalent interactions for systems with high K_a values. Compare (Fig. 4a,b and Extended Data Fig. 2) UV–vis spectroscopic and electrochemical analyses in relation to their sensitivity to variations in K_a values. Setting [C]$_0$ to be 1 mmol L^{-1}, the UV–vis spectroscopic absorptions are sensitive to K_a values in the range of 10^2–10^4 M^{-1}. In contrast, electrochemical signals are more sensitive to the systems with high K_a values, particularly for those values

greater than 10^3 M^{-1}. For example, with [C]$_0$ set to be 1 mmol L^{-1}, the two theoretical UV–vis titration curves ($K_a = 10^5$ and 10^6 M^{-1}) reproduced in Fig. 4c are nearly identical, while the two theoretical electrochemical titration curves ($K_a = 10^5$ and 10^6 M^{-1}) are clearly distinguishable. In the case of UV–vis titrations during K_a measurements, although their accuracy can be improved theoretically by reducing [C]$_0$, the relative error of absorbance also increases considering the relatively low molar extinction coefficient of this host–guest system. Thus, for several host–guest systems (with low molar extinction coefficients and high K_a values), electrochemical methods can provide more reliable K_a values.

Besides measuring binding constants (K_a values), electrochemical analysis can provide additional information, including the diffusion coefficient (D), the guest/host stoichiometric ratio (p) and the equilibrium potential gap of two single-electron transfer processes ($\Delta\varphi_{\beta\alpha}{}^{\ominus} = \varphi_\beta{}^{\ominus} - \varphi_\alpha{}^{\ominus}$), which are embodied, respectively, in the peak heights[29], positions[30] and shapes[31] of the CV curves (Fig. 4d). Among them, $\Delta\varphi_{\beta\alpha}{}^{\ominus}$ is the equilibrium potential gap between single-electron transfer processes α (C^{4+} + e$^-$ = C$^{2+(\bullet+)}$) and β (C$^{2+(\bullet+)}$ + e$^-$ = C$^{2(\bullet+)}$).
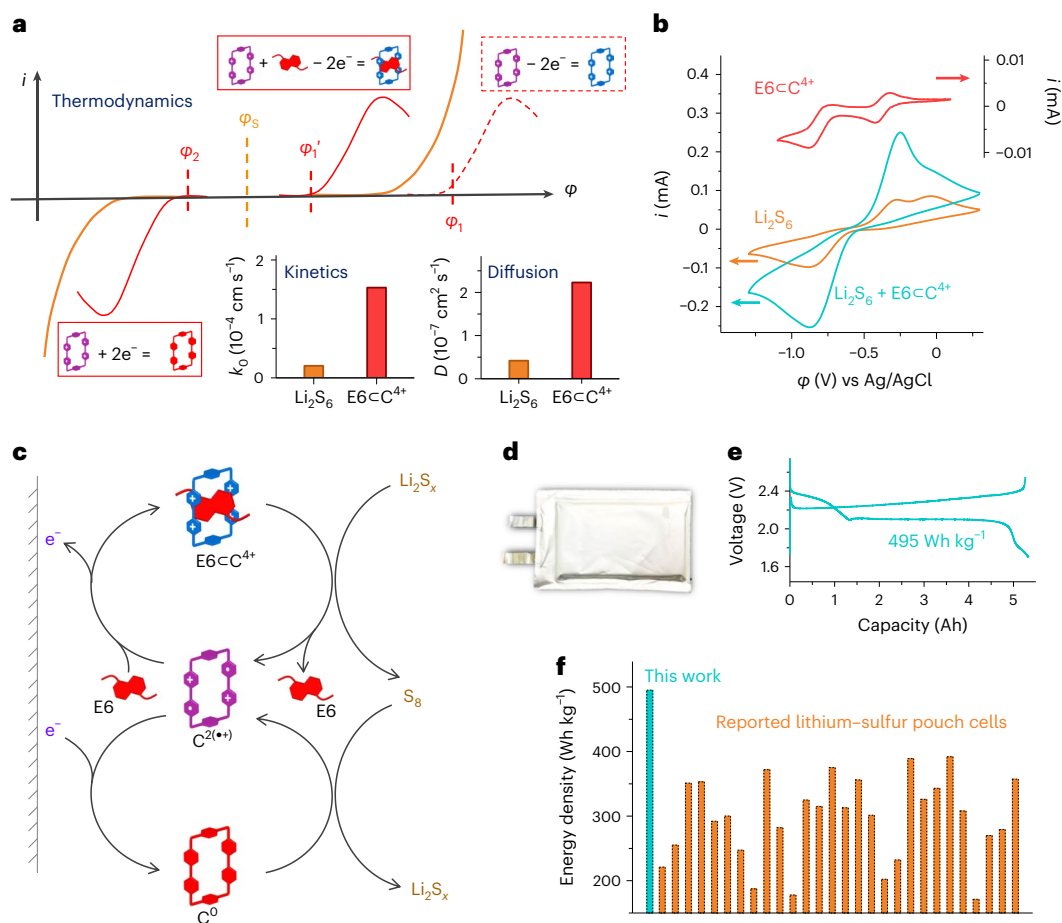
Fig. 5 | Applications in working batteries. a, Three designing/screening criteria of homogeneous catalysts for sulfur redox reactions, namely viable thermodynamics, favorable kinetics and efficient diffusion. The i–φ diagram shows the volt–ampere curves for sulfur redox (orange line), a competent homogeneous catalyst (solid red line), and $C^{4+}/C^{2(•+)}$ without the addition of En (dashed red line). Specifically, the addition of E6 reduces the redox potential of $C^{4+}/C^{2(•+)}$ (from the dashed red line into the solid red line) to satisfy the first designing/screening criterion, making E6⊂C^{4+} a competent homogeneous catalyst. The insets show the k_0 (left) and D (right) data for Li$_2$S$_6$ and E6⊂C^{4+}, indicating the satisfaction of the second and third designing/screening criteria.

b, CV curves of E6⊂C^{4+} (catalytic amount, 1 mM), Li$_2$S$_6$ (10 mM) and their mixture (10 mM Li$_2$S$_6$ + 1 mM E6⊂C^{4+}). The higher current responses for the sulfur species redox reactions with the addition of E6⊂C^{4+} demonstrate the remarkable catalytic activity of E6⊂C^{4+}. **c**, Schematic of the catalytic mechanism of E6⊂C^{4+} for the sulfur redox reaction, including charging (upper cyclic reaction path) and discharging (lower cyclic reaction path) processes. **d,e**, Photograph (**d**) and galvanostatic discharge/charging profiles obtained at the initial discharging/charging process (**e**) of the lithium–sulfur pouch cell using E6⊂C^{4+} as a homogeneous catalyst. **f**, Comparison of the energy density of the rechargeable lithium–sulfur pouch cell in this work (cyan) and values reported in the literature (orange).

Electrochemical curves offer a wealth of information pertaining to complexes. By processing and analysing electrochemical data, multiple properties of complexes can be obtained. For instance, the application of linear regression to the peak current resulting from the electrochemical reduction in relation to the CV scan rates enables the determination of D for the complexes. Notably, as the length of the oligoethylene glycol chains in En is extended, the initial augmentation of D rises from the elevated complex–solvent affinity, in going from E0 to E2. Subsequently, in going from E2 to E6, a decline in D is observed because of the increase in molecular weight. Furthermore, using curve-fitting techniques for the electrochemical titration curve, the stoichiometric ratio of the guest–host interaction can be extracted. This approach is particularly noteworthy as it demonstrates the feasibility of investigating thoroughly even the most unfamiliar supramolecular systems, achieved as a result of the sequential analysis of stoichiometric ratios and binding constants.

The detailed principles for the measurement of noncovalent interactions can be found in Supplementary Information (Supplementary Figs. 38–42), and result in the data presented in Fig. 4e. In short, the noncovalent electrochemical method of analysis can measure several physicochemical properties of complexes. Furthermore, the proposed electrochemical analyses demonstrate (Supplementary Figs. 43–46)

excellent universality when investigating host–guest complexes possessing host/guest ratios with different noncovalent interactions in a range of solvents. As a result, the noncovalent electrochemical analytical methodology is an important complement to the current spectroscopic methods. Electrochemical analyses enrich the toolbox of comprehensive and accurate measurements in supramolecular chemistry.

Analytical noncovalent electrochemistry in batteries

Analytical noncovalent electrochemistry bridges the gap between fundamental supramolecular chemistry and its application in electrochemical engineering. In contrast to other material categories, supramolecular complexes are uniquely defined by discernible noncovalent interactions, which can be regulated meticulously via host–guest interactions to reveal the properties of the complexes. These distinctive attributes also underpin their promising potential within the realm of energy chemistry and engineering. The application of supramolecular complexes in energy electrochemical engineering, however, is still relatively limited, largely because of an insufficient understanding of the relationship between noncovalent interactions and electrochemical behavior, as well as the inability to measure these supramolecular properties accurately. Fortunately, with the advent of

analytical noncovalent electrochemistry, one can design and screen host–guest complexes towards the target of electrochemical engineering. To demonstrate this application, we explored the feasibility of using noncovalent regulation utilizing complexes as homogeneous catalysts in lithium–sulfur batteries.

Lithium–sulfur batteries are amongst the next generation of energy-storage devices[32,33] as a consequence of their ultrahigh theoretical energy density (2,600 Wh kg^{-1}), which is around ten times larger than that of their current lithium-ion counterparts. The redox behavior of sulfur species in cathodes, however, is sluggish when it comes to kinetics[34], restricting the battery performance. Homogeneous catalysts (also commonly referred to as redox mediators) in lithium–sulfur batteries undergo reversible redox reactions to set up chemical–electrochemically coupled circular reactions as the bypass and thus catalyse the charging/discharging processes[35,36]. In the search for a good homogeneous catalyst for sulfur redox, three criteria must be met. (1) Viable thermodynamics: when catalysing the discharging process, the equilibrium potential of the catalyst should be slightly lower than that of the sulfur species (φ_S, the equilibrium potential of the polysulfide redox reaction) to ensure the occurrence of the chemical reaction while minimizing the overpotential[37]. The opposite is true for the charging process[38]. (2) Favorable kinetics: fast redox kinetics associated with the catalyst ensure favorable catalytic cycles[39]. (3) Efficient diffusion: the catalyst should be efficient when it comes to shuttling between the electrode surfaces and bulk-phase electrolytes[40] to activate the inert sulfur species. The screening/design of homogeneous catalysts in lithium–sulfur batteries presents a multitude of stringent demands. A single species other than a supramolecular complex makes it challenging to fulfill all of these requirements. By contrast, supramolecular complexes introduce another dimension of noncovalent interactions, holding the promise of addressing the aforementioned requirements precisely and thereby enabling the selection of optimal homogeneous catalysts.

The host C^{4+} encompasses two distinct redox processes involving C^{4+}/C$^{2(+)}$ and C$^{2(+)}$/C^0 transitions. These two redox couples ensure the catalytic capability of C^{4+} for both polysulfide oxidation (which requires C^{4+}/C$^{2(+)}$) and polysulfide reduction (which requires C$^{2(+)}$/C^0). Whereas the latter redox transformation (C$^{2(+)}$/C^0, φ_2) aligns with the criterion of viable thermodynamics that are suitable for catalysing the polysulfide reduction, the former redox transition (C^{4+}/C$^{2(+)}$, φ_1) falls short of the viable thermodynamics criterion because of its significantly elevated equilibrium potential in comparison with φ_S. Our inspiration stems from the principles of analytical noncovalent electrochemistry, which advocate the introduction of noncovalent interactions to tailor redox potentials. By engaging species that are capable of interacting selectively with C^{4+} through appropriate K_a values, it becomes possible to reduce the equilibrium potential of C^{4+}/C$^{2(+)}$ with precision to achieve a desired value (slightly exceeding φ_S). To this end, our approach involves the utilization of E6, a guest that exhibits pronounced noncovalent interactions with C^{4+}, forming an E6⊂C^{4+} complex, while exhibiting minimal interactions with C$^{2(+)}$ or C^0. During noncovalent modulation, φ_1 is effectively tuned to a suitable value of φ_1' (marginally higher than φ_S), while φ_2 is cautiously maintained slightly below φ_S (Fig. 5a). In this context, E6 functions as a co-catalyst (Extended Data Fig. 3) that effectively modulates the properties of C^{4+}. The E6⊂C^{4+} complex thus formed serves as a pivotal catalyst in operational lithium–sulfur batteries. Furthermore, the evaluation of the reaction rate constant (k_0) and diffusion coefficient (D) reveals that E6⊂C^{4+} outperforms sulfur entities by a factor of 7.5 and 5.3, respectively (Fig. 5a inset and Supplementary Figs. 50–52).

Unsurprisingly, because it meets all of the screening criteria of viable thermodynamics, favorable kinetics and efficient diffusion, E6⊂C^{4+} does exert a striking bifunctional catalytic effect on the reduction and oxidation of sulfur species, represented by the strengthened CV current responses (Fig. 5b and Supplementary Figs. 53–57). In the case of the discharging process, the redox couple C$^{2(+)}$/C^0 sets up a reduction cyclic bypass (Fig. 5c), facilitating reduction of the sulfur species. For the charging process, E6 serves as a co-catalyst and modulates the electrochemical properties of the C^{4+}/C$^{2(+)}$ couple (Fig. 5c and Extended Data Fig. 3). They work together to set up an oxidation cyclic bypass and strengthen the oxidation of polysulfide. The catalytic effect was also confirmed in working lithium–sulfur batteries. The specific capacities are improved by 237% (2.0C) and 24.6% (0.5C) with E6⊂C^{4+} as the catalyst in coin cells following routine and high sulfur loading, respectively (Supplementary Fig. 58). The catalytic effect is also long-lasting and provides a stable capacity enhancement in long-term cycling (Supplementary Fig. 60). More impressively, using the E6⊂C^{4+} catalyst, a 5.34 Ah lithium–sulfur pouch cell (Fig. 5d) delivers a high energy density of 495 Wh kg^{-1} (Fig. 5e), an enhancement in comparison with previously documented[41–43] rechargeable lithium–sulfur pouch cells (Fig. 5f). In summary, noncovalent electrochemistry effectively serves as a bridge between noncovalent chemistry and electrochemistry. Electrochemistry affords a new perspective for measuring precisely the properties of noncovalent interactions. Conversely, the management of noncovalent interactions has emerged as a pivotal regulating dimension, bolstering the realm of energy electrochemical engineering. The exceptional catalytic prowess and the impressive battery performance demonstrated in this sector underscore the efficacy of analytical noncovalent electrochemistry in real-world applications. This achievement stands as a testament to the potency of noncovalent electrochemical approaches in addressing practical challenges.

Discussion

The noncovalent electrochemical method of analysis, which constitutes a characterization tool for noncovalent interactions, possesses several advantages. (1) Universality: compared with spectroscopic analyses that rely on specific chemical probes to show spectroscopic responses, most of the groups that participate in noncovalent interactions are electrochemically active as long as the potential range is broad enough. Electrochemical analyses can be expanded to cover more types of noncovalent interaction. (2) Accuracy: the logarithmic relations ensure a better accuracy for K_a measurements when evaluating noncovalent systems with large K_a values. (3) Efficiency: noncovalent electrochemical analysis is a method that enables a thorough investigation of host–guest chemistry, which holds promise for practical applications. It should be noted that the noncovalent electrochemical method of analysis is not a panacea since detailed structural information cannot be deduced directly. By combining different characterization techniques and even developing electrochemistry–spectroscopy devices, comprehensive structural and physicochemical properties can be obtained to deepen our insights into sophisticated noncovalent interactions in the near future.

In conclusion, we propose an electrochemical method of analysis for investigating noncovalent interactions. Compared with traditional characterization methods, electrochemistry breaks through the limitations of structure-reliance and concentration-linear correlations, leading to irreplaceable advantages in universality, accuracy and efficiency. Using this strategy, a 2:1 host–guest complex was discovered, K_a values and other diversified properties of various complexes were measured and a high-performance supramolecular homogeneous catalyst was screened to achieve a breakthrough in the energy density of batteries. These cases serve as a demonstration of the potential of interdisciplinarity between supramolecular chemistry and analytical electrochemistry. With continuing efforts in research, we believe that analytical noncovalent electrochemistry will provide us with incentives in emerging applications in the fields of instrumental analysis, bioengineering and energy technology.

Methods

Electrochemical evaluation

The electrochemical evaluation was carried out using a three-electrode system controlled using a Reference 600 multipurpose

instrument (Gamry Instruments) interfaced to a personal computer to record the CV and DPV data. The counter electrode and the reference electrode were a platinum wire electrode and a saturated Ag/AgCl electrode, respectively. The working electrode was a glassy carbon electrode with a diameter of 3.0 mm. The area of the working electrode was $0.071\ cm^2$. The surface of the working electrode was polished routinely using $0.05\ \mu m$ alumina/water slurry on a felt surface immediately before use. All the electrochemical evaluations were performed at room temperature and in N_2-purged electrolytes. The role of N_2 is to avoid the interference of electrochemical oxygen reduction reactions, as well as to protect the formed oxygen-sensitive $C^{2(\bullet+)}$ and C^0. The supporting electrolyte was $TBAPF_6$ with MeCN as the solvent. The concentration of the supporting electrolytes was 0.1 M. For the CV experiments, unless stated otherwise, the scan rate was set to $100\ mV\ s^{-1}$. Each CV measurement included three scan cycles and the second scan was plotted.

Electrochemical titration curve

	C^{4+}	+	En	$\rightleftarrows$	$En \subset C^{4+}$
Initial concentration	$[C]_0$		$[En]_0$		0
Equilibrium concentration	$[C^{4+}]$		$[En]_{eq}$		$[En \subset C^{4+}]$

Ignoring the volume change during the electrochemical titrations, we have

$$[En \subset C^{4+}] = [En]_0 - [En]_{eq} \tag{1}$$

$$[En \subset C^{4+}] = [C]_0 - [C^{4+}]. \tag{2}$$

The binding constant K_a can be expressed as

$$K_a = \frac{\left[En \subset C^{4+} \right]}{[C^{4+}][En]_{eq}}. \tag{3}$$

We define

$$x = [En]_0 / [C]_0, \tag{4}$$

where x is a quantitative indicator to describe the titrated En equivalent, reflecting the titration process.

Rearranging the above equations, we have

$$[C^{4+}] = \frac{(1-x)[C]_0}{2}$$
$$-\frac{1}{2K_a} + \frac{1}{2}\sqrt{[C]_0^2 x^2 + \left(\frac{2[C]_0}{K_a} - 2[C]_0^2\right)x + \left([C]_0 + \frac{1}{K_a}\right)^2} \tag{5}$$

$$\left[En \subset C^{4+}\right] = \frac{1}{2K_a} + \frac{(x+1)[C]_0}{2}$$
$$-\frac{1}{2}\sqrt{[C]_0^2 x^2 + \left(\frac{2[C]_0}{K_a} - 2[C]_0^2\right)x + \left([C]_0 + \frac{1}{K_a}\right)^2}. \tag{6}$$

According to the Nernst equation, the potential shift ($\Delta\varphi$) at different titration stages can be expressed as

$$\Delta\varphi = \frac{RT}{zF} \times \ln\left(\frac{[C]_0}{[C^{4+}]}\right), \tag{7}$$

where R is the gas constant ($R = 8.314\ J\ K^{-1}\ mol^{-1}$), T is the temperature ($T = 298.15\ K$), z is the electron transfer number ($z = 2$ herein) and F is the Faraday constant ($F = 96,485\ C\ mol^{-1}$).

Substituting equation (5) into equation (7) and rearranging gives

$$\Delta\varphi = -\frac{RT}{zF} \times \ln\left(\frac{(1-x)}{2} - \frac{1}{2[C]_0 K_a}\right.$$
$$\left. + \frac{1}{2}\sqrt{x^2 + \left(\frac{2}{[C]_0 K_a} - 2\right)x + \left(1 + \frac{1}{[C]_0 K_a}\right)^2}\right). \tag{8}$$

Accordingly, for the electrochemical titration with fixed $[C]_0$, $\Delta\varphi$ is a function of two independent variables including the titration process ($x = [En]_0/[C]_0$) and K_a. That is, after plotting and fitting the $\Delta\varphi$–$[En]_0/[C]_0$ data, the binding constant K_a of the supramolecular complex can be obtained.

Electrochemical titration

The electrochemical titration instrument was identical to that of the electrochemical evaluation device but with a micro-syringe installed to inject the En feedstock solution into the electrolyte. Electrochemical titrations were performed in N_2-purged MeCN solutions with 0.1 M $TBAPF_6$ as the supporting electrolyte. A continuous N_2 flow ensures an oxygen-free environment and the consequent stability of the oxygen-sensitive $C^{2(\bullet+)}$ and C^0 species. The C^{4+} solution ($[C]_0 = 1\ mM$) was placed in the container and the En feedstock solution ($[En]_{stock} = 50\ mM$) was drawn into the syringe in advance. The titrated En equivalent was controlled via regulating the injection volume of the En feedstock solution. CV and DPV evaluations were performed for each titration step. The measurement of $\Delta\varphi$ at different titration steps is based on the peak position changes.

X-ray crystallography characterization

To grow single crystals of $E2 \subset 2C^{4+}$, a MeCN solution of $C \cdot 4PF_6$ (10 mM) and $E2$ (2 mM) was filtered and thereafter subjected to slow vapor diffusion of $^iPr_2O$ over one week, which afforded crystals suitable for X-ray crystallographic analysis. A suitable crystal was selected and the crystal was mounted on a crystal holder (MiTiGen) in paratone oil, and an XtaLAB Synergy R, DW system, HyPix diffractometer was used for data collection. The crystal was kept at 100.00(10) K during data collection. The structure was solved using OLEX2 (ref. 44) with the SHELXT structure solution program[45] using intrinsic phasing, and it was refined with the SHELXL refinement package[46] using least squares minimization.

Data availability

The data that support the findings of this study are available within the paper and its Supplementary Information files. Crystallographic data for the structure reported in this article have been deposited at the Cambridge Crystallographic Data Centre, under deposition number CCDC 2267283. A copy of the data can be obtained free of charge via https://www.ccdc.cam.ac.uk/structures/. Source data are provided with this paper.

Code availability

Custom code used in this study is available within the Supplementary Information files.

References

1. Watson, J. D. & Crick, F. H. C. Molecular structure of nucleic acids: a structure for deoxyribose nucleic acid. *Nature* **171**, 737–738 (1953).
2. Rossetti, G. et al. The structural impact of DNA mismatches. *Nucleic Acids Res.* **43**, 4309–4321 (2015).
3. Fersht, A. R. et al. Hydrogen-bonding and biological specificity analysed by protein engineering. *Nature* **314**, 235–238 (1985).
4. Johnson, E. R. et al. Revealing noncovalent interactions. *J. Am. Chem. Soc.* **132**, 6498–6506 (2010).

5. Zhang, L. et al. An electric molecular motor. *Nature* **613**, 280–286 (2023).
6. Feringa, B. L. The art of building small: from molecular switches to motors (Nobel Lecture). *Angew. Chem. Int. Ed.* **56**, 11059–11078 (2017).
7. Sauvage, J.-P. From chemical topology to molecular machines (Nobel Lecture). *Angew. Chem. Int. Ed.* **56**, 11080–11093 (2017).
8. Stoddart, J. F. Mechanically interlocked molecules (MIMs)—molecular shuttles, switches, and machines (Nobel Lecture). *Angew. Chem. Int. Ed.* **56**, 11094–11125 (2017).
9. Fan, C., Wu, W., Chruma, J. J., Zhao, J. & Yang, C. Enhanced triplet–triplet energy transfer and upconversion fluorescence through host–guest complexation. *J. Am. Chem. Soc.* **138**, 15405–15412 (2016).
10. Deutman, A. B. C. et al. Squaring cooperative binding circles. *Proc. Natl Acad. Sci. USA* **106**, 10471–10476 (2009).
11. Bissell, R. A., Cordova, E., Kaifer, A. E. & Stoddart, J. F. A chemically and electrochemically switchable molecular shuttle. *Nature* **369**, 133–137 (1994).
12. Hein, R., Beer, P. D. & Davis, J. J. Electrochemical anion sensing: supramolecular approaches. *Chem. Rev.* **120**, 1888–1935 (2020).
13. Kaifer, A. E. in *Comprehensive Supramolecular Chemistry* Vol. 8 (eds Ripmeester, J. A. & Davies J. E. D.) (Pergamon, 1996)
14. Schneider, H.-J. & Yatsimirsky, A. K. Selectivity in supramolecular host–guest complexes. *Chem. Soc. Rev.* **37**, 263–277 (2008).
15. Constable, E. C. et al. in *Comprehensive Supramolecular Chemistry* Vol. 9 (eds Sauvage, J.-P. & Hosseini, M. W.) (Pergamon, 1996)
16. Connors, K. A. *Binding Constants: The Measurement of Molecular Complex Stability* (Wiley, 1987)
17. Thordarson, P. Determining association constants from titration experiments in supramolecular chemistry. *Chem. Soc. Rev.* **40**, 1305–1323 (2011).
18. Parker, C. A. & Rees, W. T. Fluorescence spectrometry. A review. *Analyst* **87**, 83–111 (1962).
19. Patterson, M. et al. Disorder-induced incoherent scattering losses in photonic crystal waveguides: Bloch mode reshaping, multiple scattering, and breakdown of the Beer–Lambert law. *Phys. Rev. B* **80**, 195305 (2009).
20. Aurbach, D., McCloskey, B. D., Nazar, L. F. & Bruce, P. G. Advances in understanding mechanisms underpinning lithium–air batteries. *Nat. Energy* **1**, 16128 (2016).
21. Xie, J. et al. Spatial and kinetic regulation of sulfur electrochemistry on semi-immobilized redox mediators in working batteries. *Angew. Chem. Int. Ed.* **59**, 17670–17675 (2020).
22. Trabolsi, A. et al. Radically enhanced molecular recognition. *Nat. Chem.* **2**, 42–49 (2010).
23. Odell, B. et al. Cyclobis(paraquat-*p*-phenylene). A tetracationic multipurpose receptor. *Angew. Chem. Int. Ed.* **27**, 1547–1550 (1988).
24. Jiao, Y. et al. Electron-catalysed molecular recognition. *Nature* **603**, 265–270 (2022).
25. Choi, J. W. et al. Ground-state equilibrium thermodynamics and switching kinetics of bistable [2]rotaxanes switched in solution, polymer gels, and molecular electronic devices. *Chem. Eur. J.* **12**, 261–279 (2006).
26. Frasconi, M. et al. Redox control of the binding modes of an organic receptor. *J. Am. Chem. Soc.* **137**, 11057–11068 (2015).
27. Castro, R., Nixon, K. R., Evanseck, J. D. & Kaifer, A. E. Effects of side arm length and structure of *para*-substituted phenyl derivatives on their binding to the host cyclobis(paraquat-*p*-phenylene). *J. Org. Chem.* **61**, 7298–7303 (1996).
28. Venturi, M., Dumas, S., Balzani, V., Cao, J. G. & Stoddart, J. F. Threading/dethreading processes in pseudorotaxanes. A thermodynamic and kinetic study. *New J. Chem.* **28**, 1032–1037 (2004).
29. Nicholson, R. S. & Shain, I. Theory of stationary electrode polarography. Single scan and cyclic methods applied to reversible, irreversible, and kinetic systems. *Anal. Chem.* **36**, 706–723 (1964).
30. Bard, A. J., Faulkner, L. R. & White, H. S. *Electrochemical Methods: Fundamentals and Applications* (Wiley, 2022)
31. Polcyn, D. S. & Shain, I. Multistep charge transfers in stationary electrode polarography. *Anal. Chem.* **38**, 370–375 (1966).
32. Conder, J. et al. Direct observation of lithium polysulfides in lithium–sulfur batteries using operando X-ray diffraction. *Nat. Energy* **2**, 17069 (2017).
33. Zhao, C. et al. A high-energy and long-cycling lithium–sulfur pouch cell via a macroporous catalytic cathode with double-end binding sites. *Nat. Nanotechnol.* **16**, 166–173 (2021).
34. Yuan, Z. et al. Powering lithium–sulfur battery performance by propelling polysulfide redox at sulfiphilic hosts. *Nano Lett.* **16**, 519–527 (2016).
35. Tamirat, A. G., Guan, X., Liu, J., Luo, J. & Xia, Y. Redox mediators as charge agents for changing electrochemical reactions. *Chem. Soc. Rev.* **49**, 7454–7478 (2020).
36. Cao, D. et al. Threshold potentials for fast kinetics during mediated redox catalysis of insulators in Li–O_2 and Li–S batteries. *Nat. Catal.* **5**, 193–201 (2022).
37. Gerber, L. C. H. et al. Three-dimensional growth of Li_2S in lithium–sulfur batteries promoted by a redox mediator. *Nano Lett.* **16**, 549–554 (2016).
38. Tsao, Y. et al. Designing a quinone-based redox mediator to facilitate Li_2S oxidation in Li–S batteries. *Joule* **3**, 872–884 (2019).
39. Zhao, M. et al. Dictating high-capacity lithium–sulfur batteries through redox-mediated lithium sulfide growth. *Small Methods* **4**, 1900344 (2020).
40. Meini, S., Elazari, R., Rosenman, A., Garsuch, A. & Aurbach, D. The use of redox mediators for enhancing utilization of Li_2S cathodes for advanced Li–S battery systems. *J. Phys. Chem. Lett.* **5**, 915–918 (2014).
41. Chen, Z.-X. et al. Toward practical high-energy-density lithium–sulfur pouch cells: a review. *Adv. Mater.* **34**, 2201555 (2022).
42. Doerfler, S. et al. Challenges and key parameters of lithium–sulfur batteries on pouch cell level. *Joule* **4**, 539–554 (2020).
43. Zhou, G., Chen, H. & Cui, Y. Formulating energy density for designing practical lithium–sulfur batteries. *Nat. Energy* **7**, 312–319 (2022).
44. Dolomanov, O. V., Bourhis, L. J., Gildea, R. J., Howard, J. A. K. & Puschmann, H. *OLEX2*: a complete structure solution, refinement and analysis program. *J. Appl. Crystallogr.* **42**, 339–341 (2009).
45. Sheldrick, G. M. *SHELXT* – integrated space-group and crystal-structure determination. *Acta Crystallogr.* **A71**, 3–8 (2015).
46. Sheldrick, G. M. Crystal structure refinement with *SHELXL*. *Acta Crystallogr.* **C71**, 3–8 (2015).

Acknowledgements

Author contributions

Competing interests

The authors declare no competing interests.

Additional information

Extended data is available for this paper at https://doi.org/10.1038/s44286-024-00038-0.

Supplementary information The online version contains supplementary material available at https://doi.org/10.1038/s44286-024-00038-0.

Correspondence and requests for materials should be addressed to Qiang Zhang or J. Fraser Stoddart.

Peer review information *Nature Chemical Engineering* thanks Sang-Young Lee, and the other, anonymous, reviewer(s) for their contribution to the peer review of this work.

Reprints and permissions information is available at www.nature.com/reprints.

Publisher's note Springer Nature remains neutral with regard to jurisdictional claims in published maps and institutional affiliations.
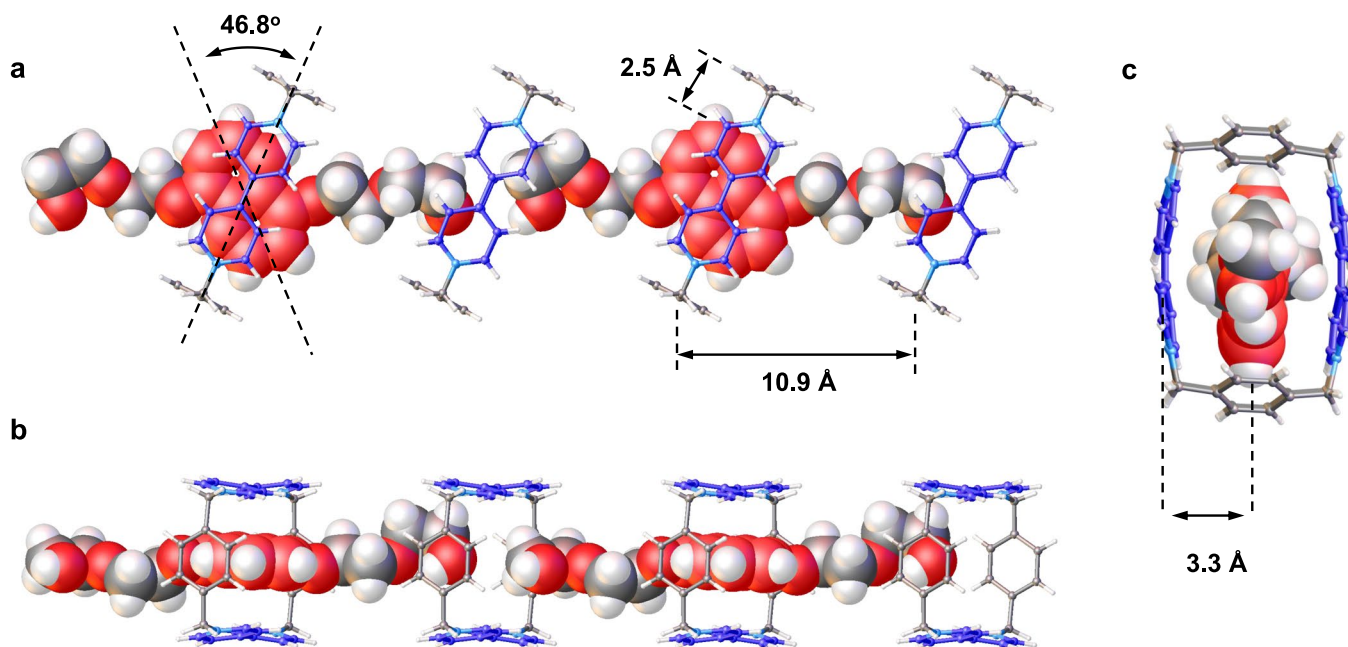
Extended Data Fig. 1 | Single-crystal superstructure of the 2:1 host–guest complex. (**a**) The front view, (**b**) the top-down view, and (**c**) the side-on view of the X-ray crystal structure of **En⊂2C⁴⁺**, whose host/guest ratio is determined to be 2:1. MeCN solvent and PF_6^- counterions are omitted for the sake of clarity.
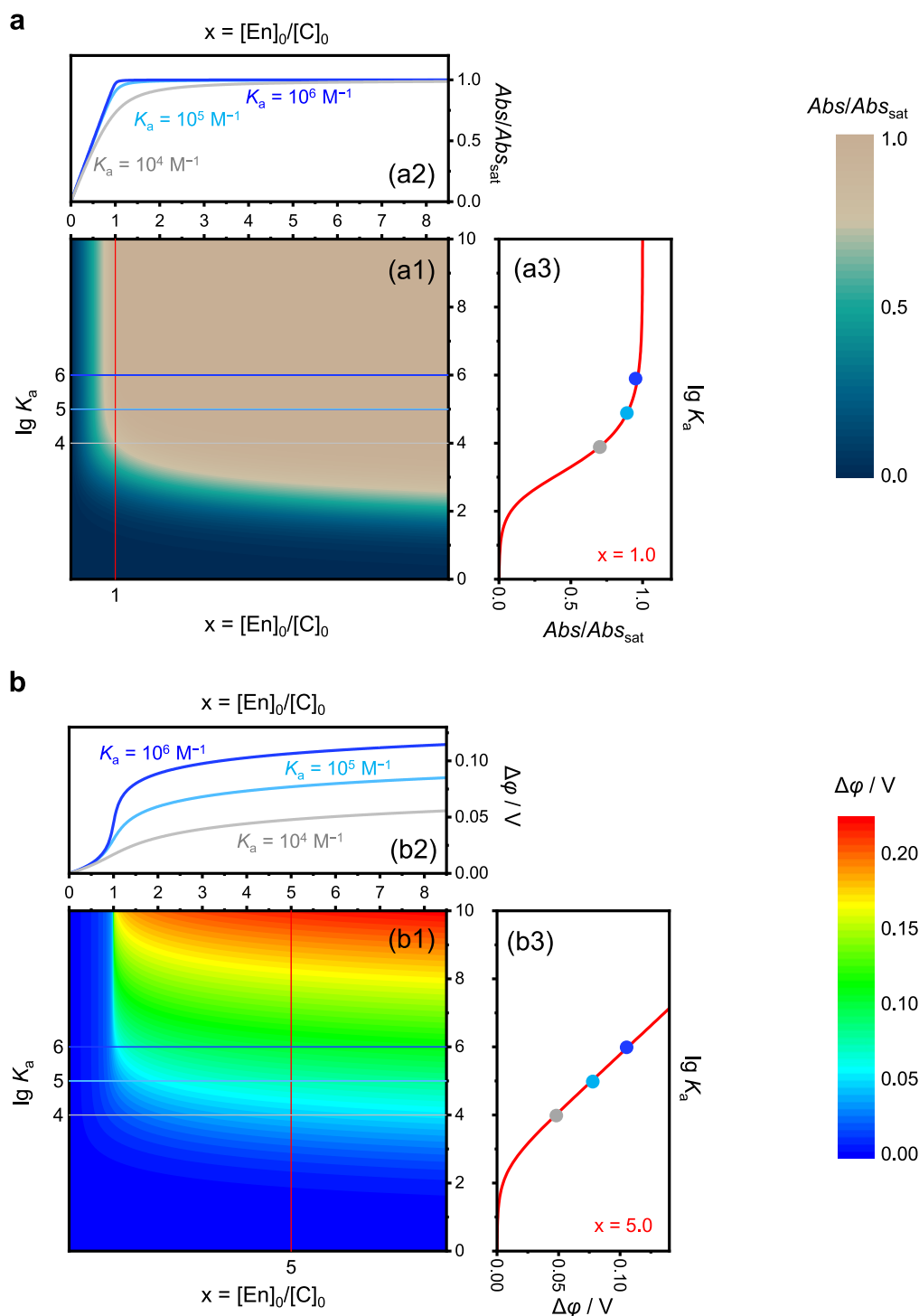
Extended Data Fig. 2 | Sensitivity analyses on UV/Vis titration and electrochemical titrations to compare their accuracy on K_a evaluation. (**a**) Normalized absorbance (Abs/Abs_{sat}) at different K_a values and different titration equivalent (x), plotting the function image of $Abs/Abs_{sat} = Abs/Abs_{sat}(x, K_a)$ (**a1**), the cross profile at $K_a = 10^4, 10^5, 10^6$ M^{-1} (**a2**), and cross profile at x = 1.0 (**a3**). The cross profile at specific K_a refers to the titration curve. The cross profile at specific x refers to the sensitivity analysis to assess the accuracy of K_a

measurements. UV/Vis titrations show little Abs/Abs_{sat} gradient when $K_a > 10^3$ M^{-1}, implying an unsatisfactory measuring accuracy. (**b**) Electrochemical signal ($\Delta\varphi$) at different K_a values and different x, exhibited as the function image of $\Delta\varphi = \Delta\varphi(x, K_a)$ (**b1**) and the sectional view at $K_a = 10^4, 10^5, 10^6$ M^{-1} (**b2**) and at x = 5.0 (**b3**). The electrochemical signal varies significantly when $K_a > 10^2$ M^{-1}, indicating higher sensitivity against different K_a values.
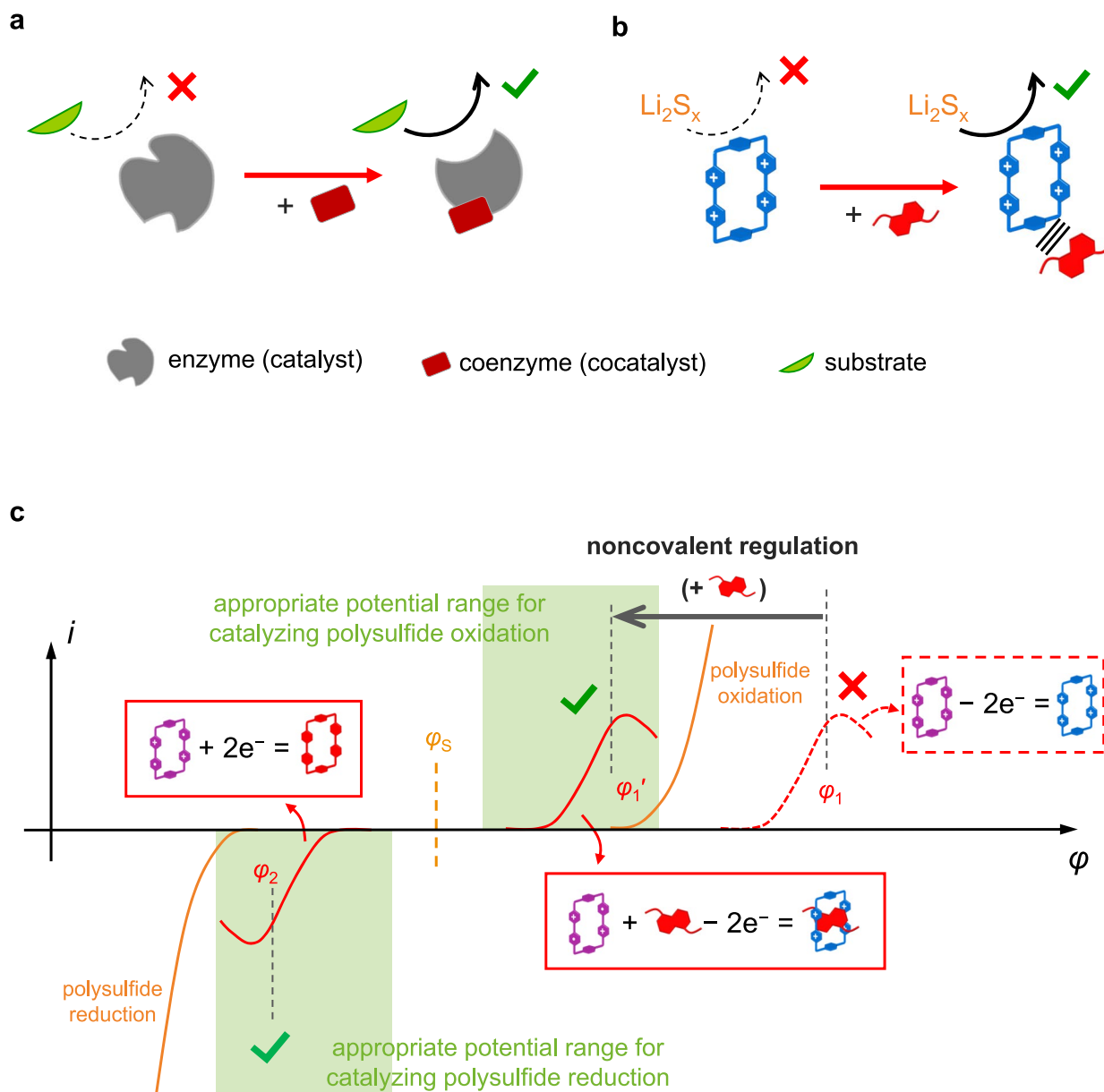
Extended Data Fig. 3 | Inspiration and guidance of analytical noncovalent electrochemistry for battery engineering. (**a**) Coenzyme Mechanism: Schematic diagram illustrating the mechanism of coenzymes. Coenzymes play a vital role in enzyme catalysis by engaging in specific chemical reactions as transient carriers of functional groups or electrons, promoting efficient catalytic processes. (**b**) Noncovalent Regulation Mechanism: Schematic representation of the noncovalent regulation mechanism. In this mechanism, the guest (**E6**) acts as a cocatalyst, activating **C⁴⁺** via noncovalent interactions. The resulting complex serves as a synergistic catalyst within operational batteries, akin to the coenzyme mechanism. (**c**) Schematic representation illustrating the mechanism of noncovalent regulation involving **E6** as a cocatalyst for the activation of **C⁴⁺**. **E6** displays specific and selective interaction with **C⁴⁺** via noncovalent binding interactions. This interaction leads to a controlled reduction in the redox potential of **C⁴⁺**, aligning with the fundamental principles of analytical noncovalent electrochemistry. Consequently, this strategic manipulation of **C⁴⁺** redox potential orchestrates its precise positioning within an optimized range. This optimized redox potential configuration is instrumental in showcasing exceptional catalytic efficacy in polysulfide oxidation process.